Propagating SST anomalies in COADS and MICOM-NERSC

Arne Melsom*, Helge Drange† and Rasmus E. Benestad*

June 15, 2001

1 Introduction

There is an increasing awareness of how oceanic teleconnections link phenomena in distant regions to each other. This was first described for the Pacific Ocean, where the strong events related to El Niño/Southern Oscillation (ENSO) have been shown to generate secondary anomalies that propagate over thousands of kilometers. Although the Atlantic Ocean lacks a momentous signal such as El Niño, a considerable variability in the equatorial Atlantic Ocean has been detected. This has been attributed to the Gulf of Guinea upwelling (the Benguela Niño, or the Atlantic El Niño) [*Adamec and O'Brien*, 1978; *Zebiak*, 1993] and the tropical Atlantic dipole [*Chang* et al., 1997].

Sutton and Allen [1997] speculate that the variability in the equatorial Atlantic Ocean is related to anomalous events in the Gulf Stream system and the North Atlantic Current. By examination of the 1945-1989 sea surface temperature (SST) anomalies [*da Silva* et al., 1994] in the North Atlantic Ocean, they discovered that the anomalies in a region off Cape Hatteras (80-60°W, 31.5-38.5°N) are correlated with SSTs along the pathway of the Gulf Stream Extension and the North Atlantic Current at lags of 0-9 years. Using a 5 year boxcar smoother, *Sutton and Allen* report that the 9 year lagged correlations reach maximum values that exceed 0.75 to the southwest of the Scotland-Iceland ridge. In this study we present results from a similar investigation, shifting the reference region from the mid-latitude western Atlantic Ocean to the region of the Scotland-Iceland ridge where the inflow of warm Atlantic water to the Nordic Seas is found. We will consider both lagged and leading correlation, hereafter, we refer to both as signed lagged correlations. Further, we will use one set of SSTs that is derived from in situ observations, and one set of mixed layer temperatures (MLTs) that is the result of a numerical model simulation. We will limit the study to the mean winter anomalies, which is a common approach for mid- and high-latitude studies.

2 Preprocessing the COADS SST data

We first consider the SST data in the Comprehensive Ocean-Atmosphere Data Set (COADS) [*Woodruff* et al., 1985], and use the 1°-by-1° monthly product, which presently covers the period from January 1960 through December 1997. The data are compiled from in situ measurements which have been taken from ships, buoys, and near-surface oceanographic profiles. The spatial coverage varies in time, and this is unfortunate in a study of spatial anomalies such as the present. Hence, the first part of the analysis of the COADS data is to obtain a set of monthly SST fields which is homogeneous in space. The preprocessing of

*Norwegian Meteorological Institute, Oslo, Norway. (arne.melsom@dnmi.no)
†Nansen Evironmental and Remote Sensing Center, Bergen, Norway. (helge.drange@nrsc.no)

the COADS SSTs was performed by requiring certain criteria to be met for a grid cell to be included in the subsequent computation of lagged correlations.

Before any anomalies can be computed, we need to establish a climatology of SSTs for the months that will be included in the study. In order to have confidence in the climatology, we will only include grid cells where observations are complete for at least a minimum number of winters. For each cell *i,j* and each month m of each winter w, set $n_{i,j}^{m,w}$=1 if there is an SST value, and =0 if no value is given. Then define

$$S^{(all)}{}_{i,j} = \sum_{w=firstwinter}^{lastwinter} \left[\prod_{mo=firstmonth}^{lastmonth} n_{i,j}^{mo,w} \right] \tag{1}$$

As an example, the study by *Sutton and Allen* [1997] encompasses data for $firstwinter =$ 1945/1946, $lastwinter =$ 1988/1989, $firstmonth = November$, and $lastmonth = April$. Here, we'll use the same definition of the winter season, and set $firstwinter =$ 1960/1961, $lastwinter =$ 1996/1997, and restrict computation of the monthly climatology to grid cells for which $S^{(all)} \geq S^{(all)}{}_{min}$. We define the COADS' mean winter SST as

$$\begin{aligned} \forall i,j \mid S^{(all)}{}_{i,j} &\geq S^{(all)}{}_{min} : \\ SST^{(winter)}{}_{i,j} &= \frac{1}{6S^{(all)}{}_{i,j}} \sum_{w='60/'61}^{'96/'97} \left[\left(\prod_{mo=Nov}^{Apr} n_{i,j}^{mo,w} \right) \sum_{m=Nov}^{Apr} SST_{i,j}^{m,w} \right] \end{aligned} \tag{2}$$

and the monthly climatology of COADS SST anomalies for the winter season may be defined as

$$\forall i,j \quad | \quad S^{(all)}{}_{i,j} \geq S^{(all)}{}_{min} :$$

$$\Delta SST_{i,j}^{m} = S^{(all)}{}_{i,j}{}^{-1} \sum_{w='60/'61}^{'96/'97} \left(\prod_{mo=Nov}^{Apr} n_{i,j}^{mo,w} \right) (SST_{i,j}^{m,w} - SST^{(winter)}{}_{i,j}) \tag{3}$$

Finally, the grid cells that don't meet the criterium for $S^{(all)}$ as defined above are filled with $SST^{(winter)}$ and ΔSST values obtained by extrapolation, using an iterative Laplacian solver.

Next, the land-sea grid is set. For each grid cell, we define the number of non-empty winter seasons as $S^{(one)}$:

$$\begin{aligned} N_{i,j}^{w} &= \max \left[(n_{i,j}^{mo,w})_{mo=firstmonth}^{lastmonth} \right] \\ S^{(one)}{}_{i,j} &= \sum_{w=firstwinter}^{lastwinter} N_{i,j}^{w} \end{aligned} \tag{4}$$

We require that all sea grid cells contain an SST value for at least one month for a number of winter seasons that exceeds or is equal to a minimum value $S^{(one)}{}_{min}$.

In order to determine the winter anomaly from one or a few months, the monthly climatology of SST anomalies must be known with some degree of confidence. We define the minimum "box distance" to an original climatology grid cell as

$$D_{i,j} = \min \left[\forall x,y \mid S^{(all)}{}_{x,y} \geq S^{(all)}{}_{min} : \max(\mid i-x \mid, \mid j-y \mid) \right] \tag{5}$$

Furthermore, we define the maximum "box distance" to an SST value in any winter season as

$$d_{i,j} = \max \left\{ \left(\min \left[\forall x,y \mid N_{x,y}^{w} = 1 : \max(\mid i-x \mid, \mid j-y \mid) \right] \right)_{w='60/'61}^{'96/'97} \right\} \tag{6}$$

Now, a grid cell that satisfies both $D < D_{min}$ and $d_{i,j} < D_{min}$, in addition to the restrictions imposed on $S^{(one)}$ above, will be considered as a sea grid in the analysis in the next section. All other grids will be flagged as land cells.

To illustrate the definitions for D (Eq. 5) and d (Eq. 6), we note that for an original climatology grid cell that has no SST values for all months in one of the winter seasons, $D_{i_1,j_1} = 0, d_{i_1,j_1} > 0$, while for a non-climatology grid cell with an SST value for one month for all winter seasons, $D_{i_2,j_2} > 0, d_{i_2,j_2} = 0$. Moreover, if these two cells are adjacent, *i.e.*, $\max(\mid i_1 - i_2 \mid, \mid j_1 - j_2 \mid) = 1$, we have $d_{i_1,j_1} = D_{i_2,j_2} = 1$. Finally, assume that ${S^{(one)}}_{i_1,j_1} \geq {S^{(one)}}_{min}$ and ${S^{(one)}}_{i_2,j_2} \geq {S^{(one)}}_{min}$. Hence, if $D_{min} \leq 1$ and $d_{min} \leq 1$, then both (i_1, j_1) and (i_2, j_2) are sea grid cells. However, if $D_{min} > 1$ and $d_{min} > 1$, these cells are both land grids.

Since we intend to analyse fields that have a time invariant land-sea grid, a procedure must be introduced in order to obtain an anomaly when data is missing in a sea grid cell for all months in one particular winter season. For each winter season w, the following procedure is applied:

1. for grid cells that satisfy $\prod_{mo=firstmonth}^{lastmonth} n_{i,j}^{mo,w} = 1$, compute the mean SST for the present winter w and subtract the overall mean value ${SST^{(winter)}}_{i,j}$
2. for the remaining grid cells that satisfy $N_{i,j}^{w} = 1$, compute the mean SST by assuming that the seasonal cycle for the present winter w is the same as the mean seasonal cycle ${SST^{(winter)}}_{i,j} + \Delta SST_{i,j}^{m}$
3. for the remaining grid cells ($N_{i,j}^{w} = 0$), extrapolate the results from steps 1. and 2. above using an iterative Laplacian solver
4. mask the land grid cells

With $firstmonth = November$ and $lastmonth = April$, the total number of winter seasons in the present COADS data set is 37. In this study, we set ${S^{(all)}}_{min} = 18$, ${S^{(one)}}_{min} = 26$, $D_{min} = 3$, $d_{min} = 1$. The mean winter SSTs ($SST^{(winter)}$, as defined in Eq. 2) with the land-sea mask that results from the present procedure and choice of parameters, are displayed in Fig. 1.

The SST data in most of the Nordic Seas are sparse, so a proper monthly climatology of SST anomalies cannot be defined here, and the data don't have the resolution that is required for a study of interannual variability. We also note that the data coverage is even more sparse in the Labrador Sea.

3 Lagged correlations of SSTs from the COADS data

We first repeat the analysis in *Sutton and Allen* [1997], who computed the lagged correlations with respect to the average of winter SSTs over the region 80-60°W, 13.5-38.5°N (off Cape Hatteras), using a 5 year low pass boxcar (LPB) smoother. Our results indicate a similar pathway of propagating SST anomalies as that in *Sutton and Allen* (see their Figure 1b). Also, the lags of maximum correlations along this pathway agree well with *Sutton and Allen*. However, we find lower correlation values and a less well-defined defined pathway. These discrepancies are due to the use of different data sets which cover only partially overlapping time periods. (*Sutton and Allen* use the NOAA SMD94 SST data [*da Silva* et al., 1994] for the period 1945-1989.) In particular, the major warm anomaly in *Sutton and Allen*'s study, which is observed during the 1950s, predates our data.

Here, we shall perform an analysis that is analogous to the *Sutton and Allen* [1997] study, with the focus of attention shifted from the western mid-latitudes of the North Atlantic Ocean to the region of inflow of warm, salty waters to the Nordic Seas, across the Scotland-Iceland

ridge. We start the analysis by computing the standard deviation of the winter SSTs. The purpose of this is to define regions were the signal-to-noise ratio is favorable, *i.e.*, where a satisfactory interannual SST signal is identifiable. From the map of winter SST standard deviations (not shown) we select two reference regions just inside the Nordic Seas, 5-2°W, 62-65°N near the Faroe Islands (NFI box) and 11-8°W, 63-66°N east of Iceland (EI box). The smoothed time series of SST winter anomalies in these two regions are depicted in Fig. 2.

From Fig. 2, we note that the winter SST anomalies in the EI box was generally lower than the NFI box anomalies in the 1960s and early 1970s, and that the rise in winter SSTs in the EI box around 1970 succeeded the corresponding rise in the NFI box. In the remaining years, the situation was generally reversed, with winter SST anomalies being higher in the EI box and the rise of EI winter SSTs in the early 1980s preceeding the rise in the NFI box. In the following, we will restrict the analysis of lagged correlations to the NFI box as the reference box. Due to the poor data coverage in the Nordic Seas, we will also restrict the discussion to negative lags, *i.e.*, winter SST anomalies that lead the NFI box anomalies. The present analysis of the COADS data is unfit to describe propagation of SST anomalies within the Nordic Seas, and we are not in a position to conduct a study such as the work by *Furevik*

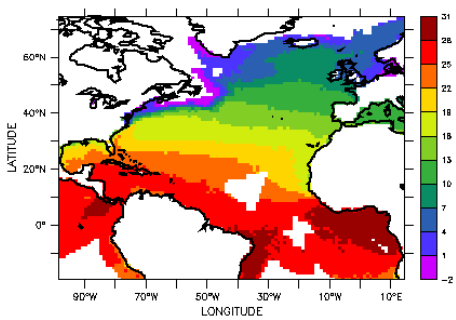

Figure 1: The COADS' mean winter (N-D-J-F-M-A) SST in the North Atlantic Ocean and bordering seas, masked according to the definitions and setting of parameter values as described in this section. The color coding of the SSTs are shown by the bar to the right, in °C.

[2000].

The lagged correlations of winter SST anomalies are displayed in Fig. 3. No well-defined pathway of propagating winter SST anomalies can be inferred from this figure. However, we note that for lags in the range -5 to 0 years, the highest correlation values is found in the immediate vicinity of the NFI box. For negative lags beyond this range, the highest correlation values are found in the region of the North Atlantic Current.

From Fig. 4, it is evident that there is a region in the vicinity of the North West Approaches (NWA) off the British Isles were the correlation values never exceed 0.6. To the south west of the NWA, maximum correlations are found at lags ≤ -5 years, while to the north east of the NWA, the highest correlations are attained for lags ≥ -1 year. (In the numerical analysis, investigation of positive lags were included.)

4 The MICOM-NERSC simulation

In this study, a global version of the Miami Isopycnic Coordinate Ocean Model MICOM [*Bleck* et al., 1992] was used to simulate the temporal and spatial variability of the SSS of the Nordic Seas. MICOM was configured with a local horizontal orthogonal grid system with one pole over North America and one pole over western part of Asia [*Bentsen* et al., 1999]. The horizontal grid resolution vary between 30 and 270 km, with about 45 km resolution in the central Nordic Seas.

The model has 24 layers in the vertical, of which the uppermost mixed layer (ML) has a temporal and spatial varying density. The specified potential densities of the sub-surface layers were chosen to ensure proper representation of the major water masses in the North Atlantic/Nordic Seas region. The densities of the isopycnic layers (in σ_0-units) are 24.12, 24.70, 25.28, 25.77, 26.18, 26.52, 26.80, 27.03, 27.22, 27.38, 27.52, 27.63, 27.71, 27.77, 27.82, 27.86, 27.90, 27.94, 27.98, 28.01, 28.04, 28.07, and 28.10.

The vertically homogeneous ML utilises the *Gaspar* [1988] bulk parameterisation for the dissipation of turbulent kinetic energy, and has temperature, salinity and layer thickness as the prognostic variables. In the isopycnic layers below the ML, temperature and layer thickness are the prognostic variables, whereas the salinity is diagnostically determined by

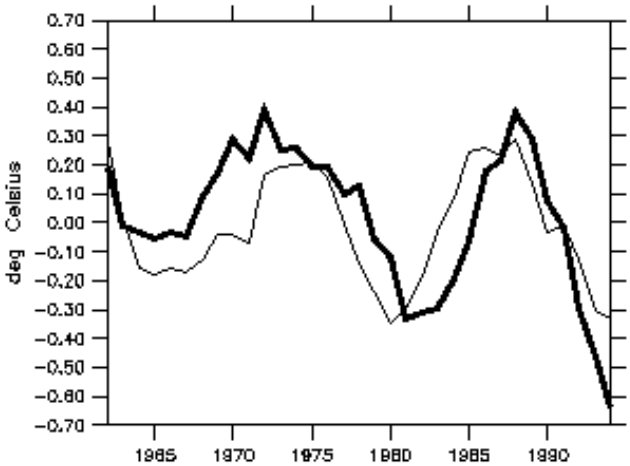

Figure 2: Time series for the SST winter anomalies, using a 5 year LPB smoother. The thick and thin lines correspond to the "Faroe Island reference box" (NFI box, 5-2°W, 62-65°N) and the "east of Iceland reference box" (EI box, 11-8°W, 63-66°N), respectively.

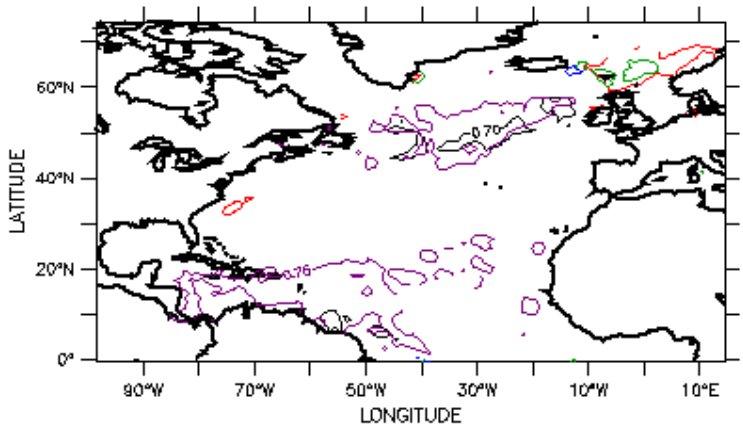

Figure 3: Contours for correlations of anomalous winter SSTs with respect to the NFI box SST anomalies, for various lags (lag 0 years: correlation value 0.6; -2 years: 0.6; -4 years: 0.6; -6 years: 0.7; -8 years: 0.75)

means of the simplified equation of state of *Friedrich and Levitus* [1972]. The bathymetry is computed as the arithmetic mean value based on the ETOPO-5 data base [*NOAA*, 1988].

The thermodynamic module incorporates freezing and melting of sea ice and snow covered sea ice *Drange and Simonsen* [1996], and is based on the thermodynamics of *Semtner* [1976], *Parkinson and Washington* [1979], and *Fichefet and Gaspar* [1988]. The dynamic part of the sea ice module is based on the viscous-plastic rheology of *Hibler* [1979], where sea ice is considered as a two-dimensional continuum. The dynamic ice module has been further modified by *Harder* [1996] to include description of sea ice roughness and the age of sea ice, and utilising the advection scheme of *Smolarkiewicz* [1984].

The continuity, momentum and tracer equations are discretized on an Arakawa C-grid stencil [*Arakawa*, 1966]. The diffusive velocities (diffusivities divided by the size of the grid

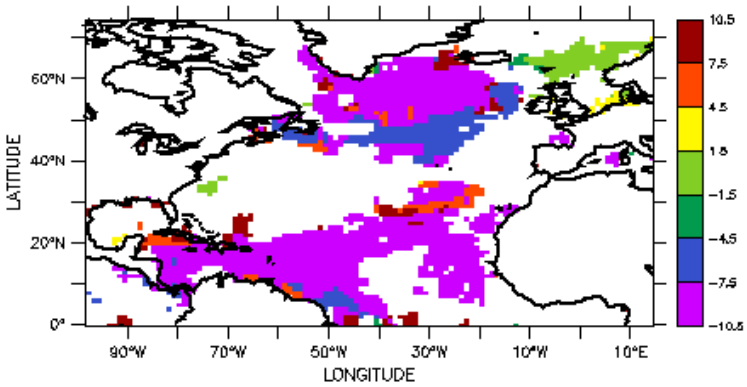

Figure 4: Lags at which the maximimum correlation values were attained, with respect to the NFI box winter SST anomalies. Lags were examined for a range of ±10 years. Only regions where the maximum lagged correlation values exceeded a value of 0.6 are shown. The color coding of the lags are indicated by the bar to the right, with numbers corresponding to lags in years.

cell) for layer interface diffusion, momentum dissipation, and tracer dispersion are 0.02 m s^{-1}, 0.025 m s^{-1} and 0.015 m s^{-1}, respectively, yielding actual diffusivities of about 10^3 m^2 s^{-1}. A flux corrected transport scheme [*Zalesak*, 1979; *Smolarkiewicz and Clark*, 1986]) is used to advect the model layer thickness and the tracer quantities.

The diapycnal mixing coefficient K_d (m^2 s^{-1}) is parameterised according to the *Gargett* [1984] expression

$$K_d = \frac{3 \times 10^{-7} \mathrm{m}^2}{N}, \tag{7}$$

where $N = \sqrt{\frac{g}{\rho}\frac{\partial \rho}{\partial z}}$ (s^{-1}) is the Brunt-Väisälä frequency. Here g (m s^{-2}) is the gravity acceleration, ρ (kg m^{-3}) is the density and z (m) is the depth. The numerical implementation of Eq. 7 follows the scheme of *McDougall and Dewar* [1998].

For the simulations discussed here, the model was initialised by the January *Levitus and Boyer* [1994] and *Levitus* et al. [1994] climatological temperature and salinity fields, respectively, a 2 m thick sea ice cover based on the climatological sea ice extent [*Lisæter* et al., 2001], and an ocean at rest. The model was then integrated for 150 years by applying the monthly mean NCAR/NCEP atmospheric forcing fields, and thereafter forced with daily NCAR/NCEP reanalysis [*Kalnay* et al., 1996] fields for the period 1948 to 1999. From the NCEP/NCAR reanalysis, wind stress, short wave, long wave, latent and sensible heat fluxes, precipitation, runoff, and sea level pressure fields are used. The momentum, heat, and fresh water fluxes are modified when the models surface state differs from the NCEP/NCAR reanalysis surface state by applying the *Fairall* et al. [1996] bulk parameterisation scheme [*Bentsen and Drange*, 2000].

During the first 150 years of the integration the ML temperature and salinity was relaxed towards the monthly mean climatological values of respectively *Levitus and Boyer* [1994] and *Levitus* et al. [1994], with a relaxation time scale of 30 days for a 50 m thick ML. The relaxation is reduced linearly with ML thicknesses exceeding 50 m, and it is set to zero in waters where sea ice is present in March (September) in the Arctic (Antarctic) to avoid relaxation towards temperature or salinity outliers in the poorly sampled polar waters. For the integration with daily fields, no relaxation of temperature was applied, whereas a fresh water flux, diagnosed from the salinity relaxation from the last years of the spin-up integration, was added to the ML.

5 Lagged correlations of SSTs from the MICOM-NERSC simulation

The results for mixed layer temperature (MLT) from the MICOM-NERSC model simulation was averaged in time with a resolution of one month. Then, the results were grouped in 1°-by-1° grid cells, and the analysis of lagged correlations become completely analogous to the analysis of the COADS SSTs above. Obviously, no preprocessing other than the grouping of model results is necessary. Again, we adopt parameter values from *Sutton and Allen* [1997], *i.e.*, we set $firstmonth = November$, $lastmonth = April$ and apply a 5 year LPB smoother to obtain $SST^{(winter)}$ and ΔSST values based on the 51 winter seasons in the simulation.

From Fig. 5, we observe that in a region off Newfoundland, the MICOM-NERSC mean winter MLTs are substantially warmer than the COADS SSTs. This is possibly due to a northward displacement of the Gulf Stream Extension in the simulation. When comparing these two sets of results, one should keep in mind that the ocean's SST and MLT will generally differ. However, we note that the MICOM-NERSC winter MLTs are generally colder than the COADS winter SSTs, and that the magnitude of this difference increases poleward. This is contrary to what one would expect, since the heat flux in the mixed layer is directed upward during winter.

We compute the standard deviation of the winter MLTs, in order to define regions were the signal-to-noise ratio is favorable. Based on the results thereof, we select two reference regions just inside the Nordic Seas, 5.5-2.5°W, 62.5-65.5°N and 11.5-8.5°W, 62.5-65.5°N. In the following, we will neglect the slight offsets when compared to the definitions in Sec. 2 of the NFI and EI boxes, respectively. The smoothed time series of MLT winter anomalies in the two regions are depicted in Fig. 6.

From Fig. 6, we note that the winter MLT anomalies in the two boxes are strongly correlated, with no obvious lags at any time during the simulation period. Hence, we will restrict the computation of lagged correlations to the NFI box being the reference region. A slight difference is seen in the amplitudes of the anomaly time series, which is somewhat larger in the NFI box. Further, we observe that there is a general trend of declining MLTs during the first half of the integration period. It is likely that this trend can be attributed to unsatisfactory quality of the NCAR/NCEP forcing.

Comparing the results displayed in the left panel of Fig. 7 with the results depicted in Figure 1b in *Sutton and Allen* [1997], we find that the "Atlantic (southern) branch" of lags in the left panel of Fig. 7 follow similar pathways in both investigations, despite the gross separation of reference boxes. Also, the propagation speed of anomalies compare favorably. As the anomalies propagate eastward from the western mid-latidues of the North Atlantic Ocean, a closer examination reveals that the anomalies in the present study are shifted somewhat, first to the north, and then to the east, when compared to *Sutton and Allen*'s results. Moreover, there are no indications of anomalies propagating into the Nordic Seas, at least not using the rather large limit for MLT correlations (0.8).

Fig. 7 and Fig. 8 contain two noteworthy features. First, we note that there is a region in the Labrador Sea for which the correlation values are of the order 0.8 for all lags that are displayed (Fig. 7). Secondly, the region were the correlation values exceed 0.8 at some lag is (impressively) large. Keeping in mind that two straight lines correlate perfectely at all lags, these features are both almost certainly related to the more than 20 year long decline in MLTs in the NFI box that ends in the early 1980s (see Fig. 6)

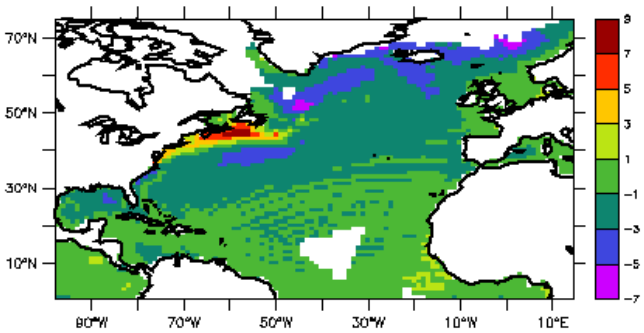

Figure 5: The difference in winter (N-D-J-F-M-A) means between COADS SSTs and MICOM-NERSC MLT in the North Atlantic Ocean and bordering seas, for the mutual sea grids (using the masking for the COADS data as described earlier) and the mutual time period (1960-1997). The color coding of the SSTs are shown by the bar to the right, in °C, with positive values corresponding to MICOM-NERSC being warmer than COADS.

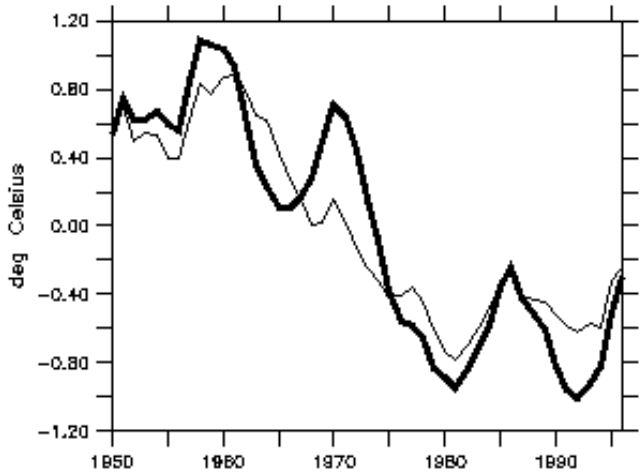

Figure 6: Time series for the MLT winter anomalies, using a 5 year LPB smoother. The thick and thin lines correspond to the "Faroe Island reference box" (NFI box, 5.5-2.5°W, 62.5-65.5°N) and the "east of Iceland reference box" (EI box, 11.5-8.5°W, 62.5-65.5°N), respectively.

6 Concluding remarks

As mentioned in Sec. 3, no well-defined pathway of propagating winter SST anomalies is found in the North Atlantic ocean in the COADS data, when the NFI winter SST anomalies serve as the reference time series. More striking is the high correlation values which occur simultaneously in the high latitude North Atlantic Ocean and south of the Sargasso Sea, for the same lags (around -10 years, see Fig. 4). This feature is possibly related to a two- or multi-pole oscillatory behavior, and such a large scale fluctuation, which is likely to have a decadal period, might well mask propagating anomalies. Hence, removal of this signal may lead to identification of propagation pathways that is more well-defined and continuous in space and time than the presentation in Sec. 3 reveals.

As a general note, the present method involving lagged correlations for the purpose of

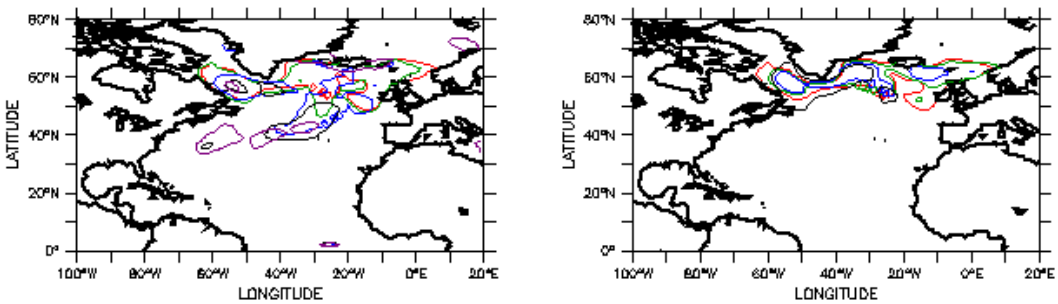

Figure 7: Contours for correlations of anomalous winter MLTs with respect to the NFI box MLT anomalies, for various lags (lag 0 years: correlation value 0.8; ±2 years: 0.8; ±4 years: 0.8; ±6 years: 0.8; -8 years: 0.75). Results for negative and positive lags are displayed in the left and right panels, respectively.

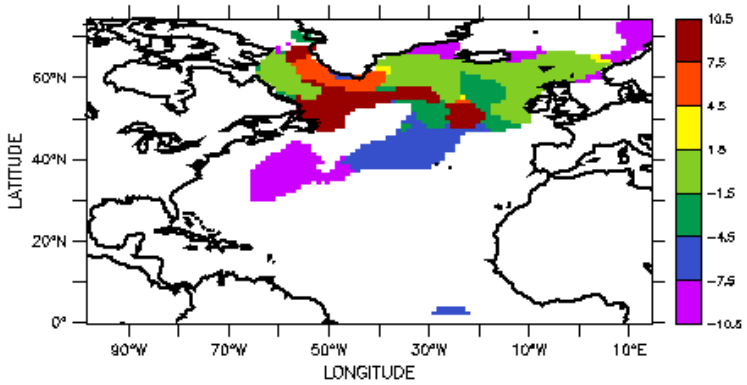

Figure 8: Lags at which the maximimum correlation values were attained, with respect to the NFI box winter MLT anomalies. Lags were examined for a range of ±10 years. Only regions where the maximum lagged correlation values exceeded a value of 0.75 are shown. The color coding of the lags are indicated by the bar to the right, with numbers corresponding to lags in years.

identification of propagating anomalies has been criticized. First, if lagged correlations are used, the linear trend should be removed prior to the analysis. Also, the use of a 5 year LPB smoother can be questioned, since the operation of smoothing individual time series has the effect of inflating the values of the cross correlation coefficients at nonzero lags [*Katz*, 1988]. Methods used for identifying the oceanic features include EOF decomposition, to which lagged regression may applied. Lagged correlation studies as well as coherence analysis can be used to identify relationships with non-zero phase difference. Two-dimensional Fast Fourier Transformation filters can be used to separate eastward propagation from westward propagation as well as identifying linear wave activity that may be associated with propagation of anomalies.

In Sec. 3, differences in the evolution of the winter SST anomalies in the NFI box and the EI box (Fig. 2) were noted. In particular, the onset of the rise in the winter SSTs was initially seen in the NFI box in the late 1960s. However, in the early 1980s another period of increasing winter SSTs is found, and now the onset is first seen in the EI box. This is possibly related to a change in the large scale atmospheric circulation. In the early 1970s, the North Atlantic Oscillation Index shifted from a negative phase to a positive phase on interannual and decedal time scales.

When comparing the results obtained for the COADS data and the MICOM-NERSC simulation, one must bear in mind the differences of these sets. These differences include method (*in situ* observations *vs.* model simulation), property (sea surface temperature *vs.* mixed layer temperature) and time period (1960-1997) *vs.* 1948-1999). This issue has been addressed in the preceeding sections, here, we repeat the note made in Sec. 3 that results using *in situ* measurements are significantly affected by including data for the 1950s.

Due to the large heat capacity of water, the MLTs are much less affected by atmospheric variability than the SSTs, except for interannual time scales and longer. Thus, for detection of propagating temperature anomalies, the MLTs make up the preferred source of information of the two. Another ocean circulation variable that should be analyzed in conjunction with the MLTs, is the thickness of the mixed layer. The product of the thickness and the MLT is a measure of the heat contained in the mixed layer, and this property is likely to be a robust measure of mixed layer temperature anomalies, and propagation thereof. However, basin-wide observations of MLT and mixed layer thickness on a decadal time scale is probably

much too sparse for a study such as the present one. Hence, validation of numerical model simulations to this end remains imperfect.

References

Adamec, D. and J. J. O'Brien, The seasonal upwelling in the Gulf of Guinea due to remote forcing, *J. Phys. Oceanogr., 8*, 1050-1060, 1978.

Arakawa, A., Computational design for long-term numerical integration of the equations of fluid motion: Two-dimensional incompressible flow. Part I. *J. Comput. Phy., 12*, 12-35, 1966.

Bentsen, M. and H. Drange, Parameterizing surface fluxes in ocean models using the NCEP/NCAR reanalysis data, *RegClim General Technical Report, 4, Norwegian Institute for Air Research, Kjeller, Norway*, pp. 149-157, 2000.

Bentsen, M. and H. Drange, Simulated formation, propagation and decay of temperature and salinity anomalies in the Atlantic Ocean, *(in prog)*, 2001.

Bentsen, M., G. Evensen, H. Drange A. D. and Jenkins, Coordinate trnasformation on a sphere using conformal mapping, *Mon. Weather Rev., 127*, 2733-2740, 1999.

Bleck, R., C. Rooth, D. Hu and L. T. Smith, Salinity-driven thermocline transients in a wind- and thermohaline-forced isopycnic coordinate model of the North Atlantic, *J. Phys. Oceanogr., 22*, 1486-1505, 1992.

Chang, P., L. Ji and H. Li, 1997, A decadal climate variation in the tropical Atlantic Ocean from thermodynamic air-sea interactions, *Nature, 385*, 516-518, 1997.

da Silva, A., C. C. Young and S. Levitus, NOAA SMD94. *Tech. Rep. 6, US Dep. Of Commerce, NOAA, NESDIS*, Washington D. C., 1994.

Drange, H. and K. Simonsen, Formulation of air-sea fluxes in the ESOP2 version of MICOM, *Technical Report 125, Nansen Environmental and Remote Sensing Center, Bergen, Norway*, 1996.

Fairall, C. W., E. F. Bradley, D. P. Rogers, J. B. Edson, and G. S. Young, Bulk parameterization of air-sea fluxes for Tropical Ocean-Global Atmosphere Coupled-Ocean Atmosphere Response Experiment, *J. Geophys. Res., 101*, 3747-3764, 1996.

Fichefet, T. and P. Gaspar, A model study of upper ocean-sea ice interaction, *J. Phys. Oceanogr., 18*, 181-195, 1988.

Friedrich, H. and S. Levitus, An approximation to the equation of state for sea water, suitable for numerical ocean models, *J. Phys. Oceanogr., 2*, 514-517, 1972.

Furevik, T., Sea surface salinity in the Nordic Seas: Climatology and variability, *J. Climate, 13* , 1044-1053, 2000.

Furevik, T., M. Bentsen, H. Drange, J. A. Johannessen and A. Korablev, On anomalous sea surface temperatures in the Nordic Seas, *J. Geophys. Res., (submitted)*, 2001.

Gao, Y., H. Drange and M. Bentsen, The Ventilation of the Intermediate and Deep Atlantic Ocean Deduced from the Spatial and Temporal Distribution of CFCs in a Global Isopycnic Coordinate Ocean Model, *Ocean Modelling (submitted)*, 2001.

Gargett, A., Vertical eddy diffusivity in the ocean interior, *J. Marine. Res., 42*, 359-393, 1984.

Gaspar, P., Modelling the seasonal cycle of the upper ocean, *J. Phys. Oceanogr., 18*, 161-180, 1988.

Harder, M., Dynamik, Rauhigkeit und Alter des Meereises in der Arktis, *PhD thesis, Alfred-Wegner-Institut fur Polar- ind Meeresforschung, Bremerhaven, Germany*, 1996.

Kalnay, E. *et al.*, The NCEP/NCAR 40-year reanalysis project, *Bull. Am. Meteor. Soc., 77*, 437-471, 1996.

Katz, R. W. *et al.*, Use of cross correlation in the search for teleconnections, *Int. J. Climatology, 8*, 241-253, 1988.

Levitus, S. and T. P. Boyer, World Ocean Atlas 1994 Volume 4: Temperature, *NOAA Atlas NESDIS 4, Washington, D.C.*, 1994.

Levitus, S., R. Burgett and T. P. Boyer, World Ocean Atlas 1994 Volume 3: Salinity, *NOAA Atlas NESDIS 3, Washington, D.C.*, 1994.

Lisaeter, K. A., O. M. Johannessen, H. Drange, G. Evensen and S. Sandven, Comparison of modeled and observed sea ice concentration and thickness fields in the Arctic, *J. Geophys. Res. (submitted)*, 2001.

McDougall, T. J. and W. K. Dewar, Vertical Mixing and Cabbeling in Layered Models, *J. Phys. Oceanogr., 28*, 1458-1480, 1998.

National Oceanic and Atmospheric Administration, Digital relief of the Surface of the Earth, *Data Ann. 88-MGG-02, NOAA, Nat. Geophys. Data Center, Boulder, CO.*, 1988.

Parkinson, C. L. and W. M. Washington, A Large-Scale Numerical Model of Sea Ice, *J. Geophys. Res., 84*, 311-337, 1979.

da Silva, A., C. C. Young and S. Levitus, NOAA SMD 94, *Tech. Rep. 6, US Dept. of Commerce, NOAA, NESDIS, Washington CD.*, 1994.

Semtner, A. J., A model for the thermodynamics growth of sea ice in numerical investigations of climate, *J. Phys. Oceanogr., 6*, 379-389, 1976.

Smolarkiewicz, P. K., A Fully Multidimensional Positive Definite Advection Transport Algorithm with Small Implicit Diffusion, *J. Comput. Phys., 54*, 25-362, 1984.

Smolarkiewicz, P. K. and T. L. Clark, The multidimensional positive definite advection transport algorithm: Further development and applications, *J. Comput. Phys., 67*, 396-438, 1986.

Sutton, R. T. and M. R. Allen, Decadal variability in North Atlantic sea-surface temperature and climate. *Nature, 388*, 563-567, 1997.

W.D. Hibler-III, A Dynamic Thermodynamic Sea Ice Model, *J. Phys. Oceanogr., 12*, 815-84, 1979.

Woodruff, S. D., H. F. Diaz, J. D. Elms and S. J. Worley, COADS Release 2 data and metadata enhancements for improvements of marine surface flux fields. *Phys. Chem. Earth, 23*, 517-527, 1985.

Zalesak, S., Fully multidimensional flux-corrected transport algorithms for fluids, *J. Comp. Physics, 31*, 335-362, 1979.